Crystal Structure of the Bowman-Birk Inhibitor from *Vigna unguiculata* Seeds in Complex with β-Trypsin at 1.55 Å Resolution and Its Structural Properties in Association with Proteinases

João Alexandre R. G. Barbosa,* Luciano P. Silva,† Rozeni C. L. Teles,‡ Gisele F. Esteves,‡ Ricardo B. Azevedo,† Manuel M. Ventura,‡ and Sonia M. de Freitas‡

*Centro de Biologia Molecular Estrutural, Laboratório Nacional de Luz Síncrotron, Campinas, Brazil; and †Laboratório de Morfologia e Morfogênese and ‡Laboratório de Biofísica, Instituto de Ciências Biológicas, Universidade de Brasília, Brasília-DF, Brazil, 70910-900

ABSTRACT The structure of the Bowman-Birk inhibitor from *Vigna unguiculata* seeds (BTCI) in complex with β-trypsin was solved and refined at 1.55 Å to a crystallographic R_{factor} of 0.154 and R_{free} of 0.169, and represents the highest resolution for a Bowman-Birk inhibitor structure to date. The BTCI-trypsin interface is stabilized by hydrophobic contacts and hydrogen bonds, involving two waters and a polyethylene glycol molecule. The conformational rigidity of the reactive loop is characteristic of the specificity against trypsin, while hydrophobicity and conformational mobility of the antichymotryptic subdomain confer the self-association tendency, indicated by atomic force microscopy, of BTCI in complex and free form. When BTCI is in binary complexes, no significant differences in inhibition constants for producing a ternary complex with trypsin and chymotrypsin were detected. These results indicate that binary complexes present no conformational change in their reactive site for both enzymes confirming that these sites are structurally independent. The free chymotrypsin observed in the atomic force microscopy assays, when the ternary complex is obtained from BTCI-trypsin binary complex and chymotrypsin, could be related more to the self-association tendency between chymotrypsin molecules and the flexibility of the reactive site for this enzyme than to binding-related conformational changes.

INTRODUCTION

Serine proteinases have diverse biological functionalities that might be harmful to other organisms different from those producing such molecules. In biological systems, they are controlled by several mechanisms including the inactivation by proteolytic degradation or by interaction with inhibitors, which act as pseudo-substrates displaying variable degrees of affinity to the enzyme's catalytic sites (1,2).

Natural inhibitors have been classified into at least 18 different families (3) among which the best studied are the serine proteinase Bowman-Birk inhibitors (BBIs) and Kunitz type inhibitors. BBIs are small and cysteine-rich serine proteinase inhibitors with a molecular mass of 6–20 kDa. They are widespread in monocotyledonous and dicotyledonous plants (4), particularly in leguminous seeds. The reactive sites are known to inhibit trypsin and chymotrypsin in monocotyledonous plants and elastase in dicotyledonous plants.

The interest in understanding the physiological significance of proteinase inhibitors has increased due to their regulating action in different processes related with proteinases. They are involved in intracellular protein breakdown, transcription, cell cycle, cell invasion, and apoptosis (5). Plant proteinase inhibitors have been described as storage proteins and as protective agents against plant infection and in plant defense processes (6,7). Soybean proteinase inhibitor has also been recognized as powerful carcinogenesis suppressor agents in animal and in vitro transformation systems and presented no adverse or toxic effects to the pancreas or to animal growth at doses up to two orders-of-magnitude higher then the doses being tested in people (8). Therefore, the structural studies of BBIs may provide novel insights on structural features and potential anticarcinogenic effects on cellular processes and in the gene expression regulation in many cancer cell lines.

Three-dimensional structures of several BBI in the free form (9–16) and in complex with trypsin (17–22) have been reported. However, no crystal structure of a Bowman-Birk inhibitor in complex with chymotrypsin has been reported, and the only structural studies on an atomic level of this complex are by molecular modeling (13,23). However, the crystallization and preliminary crystallographic information describing the crystal of BBI in complex with trypsin and chymotrypsin, without three-dimensional details, was reported before (24). All structures of BBIs are similar and have a common fold for the reactive site consisting of two distinct binding subdomains composed by a β-hairpin in an antiparallel β-sheet stabilized by disulfide bonds. The surface loops extended toward the solvent, providing easier access to the cognate enzyme's active site (22). The loops are generally very rigid, reducing the unfavorable decrease in entropy that accompanies complex formation (2,25). The change in flexibility of the loops is important to identify the internal dynamics of the binding to compare the different molecules and their affinity (26).

The most unusual structural features of BBIs are the exposed hydrophobic patches and absence of a hydrophobic core (12,20,23). This is in contrast to the hydrophobic interior

Submitted June 6, 2006, and accepted for publication October 23, 2006.

Address reprint requests to S. M. de Freitas, Tel.: 55-61-3307-2192; E-mail: nina@unb.br.

0006-3495/07/03/1638/13 $2.00

doi: 10.1529/biophysj.106.090555

and hydrophilic exterior typically observed in the majority of globular proteins. The detailed structural analysis of soybean BBI indicate the presence of these exposed hydrophobic patches, buried charged residues forming an electrically charged cluster at the interdomain boundary and internal water molecules. These structural features in the interdomain region may help stabilize the relative arrangement of the two subdomains (12). The internal water molecules were also found in pea, peanut, and mung bean BBI indicating that they are a part of the tertiary structures of these inhibitors (10,12,13,18, 19). Hydrophilic bridges and conformational rigidity of subdomain 1 in the binding region are characteristic of narrow specificity against trypsin whereas increased hydrophobicity and a significant conformational mobility are characteristic of subdomain 2. The exposed hydrophobic patches predominant in subdomain 2 seem to be responsible for the self-association of the inhibitor (12,14,20).

Most of BBIs tend to form homo or hetero-dimers, trimers, or more complex oligomers (27–29) and some of studies indicate the pivotal role of charged interactions in the case of monomer/dimer equilibria (30). The inhibitor from winter pea seeds was crystallized with a nearly perfect twofold symmetric dimmer in the asymmetric unit. Although the reactive sites of interaction with proteases are located on the surface of the dimer, it is unlikely that the dimeric form is the functional state of the molecule (13).

The black-eyed pea trypsin/chymotrypsin inhibitor (BTCI) is a Bowman-Birk type proteinase inhibitor isolated from *Vigna unguiculata* seeds presenting two different and independent reactive sites for trypsin and chymotrypsin, respectively (31). The binding of trypsin and chymotrypsin to BTCI was characterized as an endothermic, spontaneous, and entropically driven process (32,33). This inhibitor is a stable globular protein (34) with 83 residues and seven disulfide bonds (35). The binary and ternary complexes of BTCI with trypsin and chymotrypsin have been purified and extensively physicochemically characterized on the basis of hydrodynamic methods (36). Spectroscopic data on solvent perturbation and surface accessibility (35,37), light scattering (38), and the molecular homology model indicate an unusual hydrophobic surface, in contrast to standard proteins that comprise a hydrophobic core and exposed polar amino acids (23). Multimeric states of BTCI were identified from atomic force microscopy (AFM) analysis. BTCI adopts stable and well-packed self-assembled states in monomer-dimer-trimer-hexamer equilibrium with globular-ellipsoidal shapes (39). The absence of hydrophobic core and the high content of disulfide bonds result in a constrained conformation that may be responsible for the remarkable stability exhibited by this inhibitor (34), in agreement with other BBIs (12).

In this article, we present the three-dimensional structure of BTCI in complex with bovine trypsin determined by molecular replacement methods at 1.55 Å resolution and discuss the binary and ternary complexes features and the self-association tendency of these proteins by AFM experiments.

METHODS

Purification of proteins

BTCI was purified from *V. unguiculata* seeds (31). The bovine chymotrypsin was purchased from Sigma (St. Louis, MO). The bovine trypsin was purified by chromatography on a SP-Sephadex C-25-120 (Pharmacia, Peapack, NJ) from 2× crystallized trypsin (Sigma). The binary complexes (BTCI-chymotrypsin and BTCI-trypsin) were obtained by mixing BTCI and enzymes 1:1 at the concentration of 5 mM in 100 mM phosphate buffer, pH 7.4 (36) for each protein. All complexes were purified with size-exclusion chromatography.

Crystallization, data collection, and processing

Crystallization was achieved using the hanging-drop vapor diffusion method at 21°C. The crystals of BTCI-trypsin complex were grown in a droplet of 2 μL of protein solution at 8 mg/mL in sodium citrate buffer pH 4.0 and 2 μL of reservoir solution containing 0.1 M HEPES-Na buffer pH 7.5, 5% (v/v) polyethylene glycol (PEG) 400 and 2.0 M ammonium sulfate (40). The x-ray diffraction datasets were collected at the MX1-D03B beamline of the Laboratório Nacional de Luz Síncrotron (Campinas, Brazil), at $\lambda = 1.431$ Å, $\Delta\phi = 1.0°$ on a mar345 detector system. Crystals were soaked in mother solution containing 15% glycerol (v/v) as the cryoprotectant before data collection at 100 K. The diffraction data set was scaled and integrated using HKL2000 (41). The crystals were from space group $P2_12_12_1$ with cell dimensions $a = 60.50$, $b = 61.11$, and $c = 79.26$ Å, angles $\alpha = \beta = \gamma = 90.00°$. The first crystals diffracted to a resolution of 2.36 Å (40), but the best crystal was produced later, diffracting to 1.55 Å resolution.

Molecular replacement

The structure of the complex was solved by molecular replacement using the crystallographic structure of trypsin in complex with *Phaseolus angularis* BBI (17) (PDB code 1TAB) as a search model (40). A partially refined model from the first x-ray dataset at 2.36 Å resolution was used to find the molecular replacement solution for the best dataset at 1.55 Å resolution. The set of reflections used to calculate the R_{free} was kept the same for both datasets up to 2.36 Å resolution and was generated from 2.36 to 1.55 Å resolution for the higher resolution dataset. A summary of x-ray data collection statistics for the best dataset is given in Table 1.

Model building and refinement

The residues of *P. angularis* inhibitor were replaced by those of BTCI where the sequences differed using the program O (42). Initial refinement was performed using CNS (43) against the 2.36 Å resolution dataset. Using these previously refined coordinates against the 1.55 Å dataset yielded an initial R_{factor} and R_{free} of 0.265 and 0.279, respectively. At this point, the refinement program was changed to REFMAC (44) from the CCP4 (45) package. Positional refinement was alternated with model rebuilding and visualization sessions using the graphic modeling package O (42) and Coot (46). Water molecules were initially added automatically using the program ARP/wARP (47) and later by inspection of the electron density maps. The molecules of PEG, sulfate, and acetate were built into their corresponding electron densities using models from the HICUP server (48). The stereochemistry quality of this model was assessed with the PROCHECK program (49). The refinement statistics are presented in Table 1.

Structural comparisons and analysis

BTCI structural neighbors search was performed with vector alignment search tool, VAST (50). The selected BBIs three-dimensional structures

TABLE 1 X-ray data collection and refinement statistics

Data collection	
Space group	$P2_12_12_1$
Cell parameters (a, b, c) (Å)	60.50, 61.11, 79.26
Resolution range (Å)	40.00–1.55 (1.63–1.55)
Wavelength (Å)	1.431
Oscillation (°)	1.0
Detector distance (mm)	57
Number of frames	162
$I/\sigma(I)$ before merging	14.9
$I/\sigma(I)$ after merging	30.5 (4.9)
Completeness (%)	99.5 (98.6)
Redundancy	6.3(5.9)
R_{sym}*	0.060 (0.353)
Number of reflections	273,490
Number of unique reflections	43,170 (4216)
Refinement statistics	
Resolution range (Å)	30.00–1.55
Number of reflections	43111
R_{free}	2145
Number of nonhydrogen atoms	2486
Protein	2102
Water	323
Heteroatoms	61
R_{factor}†	0.154
R_{free}	0.169
RMS deviations from ideality	
Bond lengths (Å)	0.011
Bond angles (Å)	1.483
Average temperature factor (Å^2)	20.53
Protein overall (Å^2)	18.12
Solvent molecules (Å^2)	34.61
Heteroatoms (Å^2)	28.38
Ramachandran plot	
Most favored regions (%)	87.8
Additional allowed regions (%)	11.8
Generously allowed regions (%)	0.4
Overall G factor	0.1

*$R_{sym} = \Sigma\ |I - \langle I\rangle| / \Sigma\ |I|$, where $\langle I\rangle$ is the average intensity of equivalent reflections.
†$R_{factor} = \Sigma\ ||I_o| - |F_c|| / |F_o|$.

(9,11,13,14,16,21) (PDB codes: 1PI2, 1BBI, 1PBI, 1MVZ, 1H34, and 1DF9) were superimposed onto the BTCI model using the backbone atoms of the subdomains containing reactive sites with the visual molecular dynamics software (51), and the overall and reactive site's RMSD were calculated. The flexibility of the reactive site for trypsin and chymotrypsin were analyzed based on the average *B*-factor. The protein-protein interface of BTCI-trypsin complex was analyzed using the BSMPP server (52) and PyMOL program, Ver. 0.98 (53). The electrostatic potential was generated using GRASP (54).

Atomic force microscopy (AFM) measurements of BTCI-proteinases complexes

AFM measurements were carried out following the direct surface adsorption method usually applied for biomaterials, cells (55), and proteins (39). Samples of the binary and ternary BTCI-proteinase complexes and the proteinases in monomeric forms were prepared (100 μg/mL) by air-drying a 5 μL drop of stock solutions into a freshly cleaved mica surface for 20 min. All AFM experiments were carried out in the intermittent-contact mode operation on a TopoMetrix Explorer TMX 2000 atomic force microscope (TopoMetrix, Santa Clara, CA). Supertip AFM probes with curvature radius $<$20 nm mounted on cantilevers (200 μm) with a typical spring constant of 0.032 N/m were used. Scanned areas (1 μm/s speed scan) were perfect squares (1 μm $\times$ 1 μm) to which a weak force ($<$500 pN) was applied. Standard topographic intermittent contact and lateral force acquisition modes were simultaneously obtained. All AFM images contained 500 $\times$ 500 data points and the raw data images were processed and analyzed with the SPMLab 4.0 software (TopoMetrix Explorer) with only background slopes corrected. The reported lateral dimensions of surface features are the full width at half-maximum height. For control experiments, the Milli-Q water was applied onto a mica support and imaged after air-drying (Millipore, Billerica, MA). Randomly distributed contaminations in control measurements were always $<$0.5 nm in height. The accessible surface area and molecular volume were calculated as previously described for BTCI (39) using VADAR 1.4 software (56). Statistical and mathematical analyses of data were performed using ORIGIN 6.0 software.

Inhibitory activity assay of binary complexes

The inhibitory activities of the binary complexes, BTCI-trypsin and BTCI-chymotrypsin, were assayed by evaluating the chymotrypsin and trypsin activities using the substrates *n*-glutaryl-*L*-phenylalanine-*p*-nitroanilide (GPNA) and Nα-benzoyl-DL-arginine-*p*-nitroanilide (BAPNA), respectively (57). The BAPNA and GPNA were purchased from Sigma. The concentrations of the proteins used in this assay were determined from measurements of absorbance on a JASCO V-530 spectrophotometer (JASCO, Tokyo, Japan) and using the following values: trypsin (M_m = 24 kDa), $A1^{\%}_{280,1\text{-cm}} = 15.9$; chymotrypsin ($M_m$ = 24 kDa), $A1^{\%}_{280,1\text{-cm}} = 20.4$; BTCI-trypsin ($M_m$ = 25 kDa), $A1^{\%}_{280,1\text{-cm}} = 13.7$; and BTCI-chymotrypsin (M_m = 25 kDa), $A1^{\%}_{280,1\text{-cm}} = 16.8$ (58). All components of the assay were diluted in 50 mM Tris-HCl, $CaCl_2$ 20 mM pH 7.6 for chymotrypsin or pH 8.2 for trypsin residual activity measurements. The binary complexes BTCI-trypsin and BTCI-chymotrypsin used in these assays were purified as reported by Ventura et al. (36) and their concentrations varied at $\sim 10^{-6}$ and 10^{-8} M, respectively. The ternary complex was formed by incubating 250 μL of enzyme at a fixed initial concentration (28.60 μM for chymotrypsin and 2.57 μM for trypsin) with 250 μL of the binary complex lacking the enzyme in various concentrations at room temperature for 15 min. After this incubation, 1250 μL of GPNA at 0.8 mg/mL or BAPNA at 0.064 mg/mL were added. The reaction was stopped by addition of 250 μL 30% acetic acid, leading to a final volume of 2 mL.

The enzymatic hydrolysis of the substrate was evaluated by recording the absorbance at 410 nm. The residual activities of the enzymes, in the presence of the binary complexes, were estimated considering the free enzyme activity to be 100%. The obtained values are an average of three independent measurements. Inhibition curves were obtained by plotting decreasing relative activities of the chymotrypsin and trypsin versus binary complex concentration. Inhibition constants of the enzyme-inhibitor complexes, K_i, for each inhibitory assay were calculated from fitted inhibition curves following the procedure described by Morrison (59), using the GRAFIT program version 3 (Erithacus Software, Horley, Surrey, United Kingdom).

RESULTS AND DISCUSSION

Overall crystallographic structure of the BTCI-trypsin complex

Despite extensive physicochemical and structural studies of serine proteinase inhibitors, no three-dimensional structures of BBIs in complex with chymotrypsin have been reported.

Furthermore, relatively few structures in their free forms (9–16) or associated with trypsin in binary (17,21) and ternary complexes (18,20,22) have been reported. The crystal structure of the BTCI-trypsin complex was solved by molecular replacement using the crystallographic structure of trypsin in complex with *P. angularis* BBI (17) (PDB code 1TAB) as a search model. The refinement converged to a final working R_{cryst} and R_{free} factors of 0.154 and 0.169, respectively. This model represents the highest resolution structure of a BBI molecule available, 1.55 Å. All data collection, phasing, and refinement statistics are summarized in Table 1.

The final complex model includes residues 17–72 of BTCI, 16–238 of trypsin, 323 water molecules, four sulfate ions, two acetate, and three PEG molecules. The quality of the density did not allow the tracing of two segments of the BTCI (residues 1–16 and 73–83), which presumably are part of a flexible regions at the N- and C-terminus of the molecule, as reported for others BBI deposited at PDB (9,11,13,16). The model's stereochemistry quality indicated that 87.8%, 11.8%, and 0.4% of the residues are in most favored, in additional and generously allowed regions of the Ramachandran plot, respectively. No unreasonable geometry for the complex structure was found.

The BTCI structure

The overall shape of the BTCI molecule resembles an elongated cylinder with dimensions of ~42 × 22 × 18 $Å^3$. The structure of BTCI folds into two similar compact subdomains, 1 and 2, each with ~30 residues (Fig. 1). Each subdomain has three β-strands forming an antiparallel β-sheet. A striking feature of the BTCI is the presence of 14 cysteine residues that forms seven disulfide bonds. This fold is conserved in all BBIs and is easily identifiable by the cysteine pattern present in the sequence of these inhibitors as shown in the alignment in Fig. 1. Interestingly, the unusual buried cluster of charged side chains located in the intersubdomain region, previously pointed out in 1BBI (11) and 1MVZ (14), has been also identified in BTCI (Asp^{36}, Arg^{38}, and His^{43}) and in almost all structures presented in Fig. 1 *b*. In addition, the conserved Asp^{63} compose the above charged cluster making hydrogen bonds mediated by water molecules. BBIs present another cluster made of highly conserved aromatic residues (Phe^{67}, Tyr^{69}, and the His^{43} in BTCI), positioned in a typical orthogonal geometry (14). This structural feature has been described, together with the hydrogen-bond network and the seven disulfide bonds, to confer a high stability to this class of inhibitors (14,60).

Each subdomain of the BTCI contains one reactive site capable of binding to the active site of the cognate proteinase. The reactive site is formed in a conserved loop connecting two strands. The loop between strands 1 and 2 contains Lys^{26} as the P1 residue that is specific for trypsin, while the loop between strands 4 and 5 contains Phe^{53} as P1, for chymotrypsin. The distance between the Cα atoms of the two reactive sites (32.5 Å) is very similar to that of the BBIs in free form showing that there is no big changes in the overall structure upon binding. This separation allows the inhibition of two proteinase molecules simultaneously and independently (13,15,18,20,22).

The structural similarities among individual three-dimensional chains of BBIs were computed by the VAST algorithm (50). The pairwise RMSD between the identified structural neighbors and BTCI was calculated for the overall alignment and just for the antitryptic binding loop. The low RMSD values indicate that the complete structure (0.5–1.7 Å) and especially the antitryptic reactive site of the inhibitors

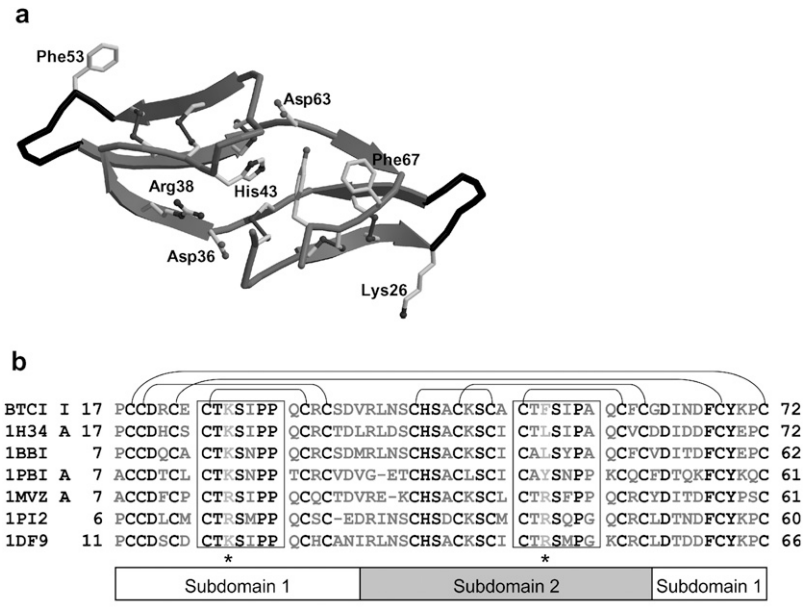

FIGURE 1 The BTCI structure. (*a*) Ribbon diagram of the BTCI structure showing disulfide bonds and P1 residues in subdomains 1 and 2 and stabilizing residues of the intersubdomain region in the BTCI structure. (*b*) Sequence alignment of representative BBIs identified by their PDB code BTCI (*V. unguiculata* seeds), 1H34 (lima bean), 1BBI (soybean), 1PBI (pea seeds), 1MVZ (snail medic seeds), 1PI2 (tracy bean), and 1DF9 (mung bean). The residues comprising the reactive loops are enclosed by boxes. The identical amino acids are represented in black, while the P1 residues are indicated by *. Subdomains 1 and 2 are indicated by open and shaded boxes underneath the alignment, respectively. The lines connecting the cysteine residues represent the disulfide bonds.

(0.06–0.75 Å) retain identical three-dimensional arrangement. Although BTCI has presented high identity with all analyzed structures (64.0–78.6%), the 1PBI, 1PI2, 1H34, and 1DF9 (crystallographic structures) have the highest structural similarity, exhibiting RMSD of 0.5–0.9 Å, whereas the 1MVZ and 1BBI (nuclear magnetic resonance (NMR) structures) have the RMSD of 1.4 and 1.7 Å, respectively. It is worth noticing the impressive RMSD of 0.06 Å for the antitryptic reactive sites of BTCI and 1H34. These results strongly indicate that BTCI exhibits the known canonical conformational typical of BBIs (25) with higher similarity to the crystallographic structures when compared with NMR ones.

Cysteine residues and the disulfide bonds they form are conserved and well defined in the electron density maps. The loops between Cys^{24}-Cys^{32}, located in the subdomain 1, and Cys^{51}-Cys^{59}, located in the subdomain 2 are the most conserved regions of BBI structures (Fig. 1). The conformational differences are in the regions that are not involved in proteinase recognition (3,15). To analyze the flexibility of the loop containing the reactive site in the BTCI, a comparison is made by plotting the average *B*-factor for each residue of the BTCI and some of the inhibitors (Fig. 2). The BTCI exhibits relatively low average overall *B*-factors (20.53 $Å^2$) when compared with other proteinase inhibitors (1H34, 1PBI, and 1DF9). The *B*-factors of the reactive site for trypsin (12.56 $Å^2$), in complex state, are much lower than the reactive site for chymotrypsin (29.07 $Å^2$), in free state, indicating that the flexibility of the inhibitor might be reduced upon complex formation. The low *B*-factors around this region are due to the involvement of these residues in extensive polar contacts with the trypsin molecule, which stabilizes the conformation of the inhibitor (Table 2).

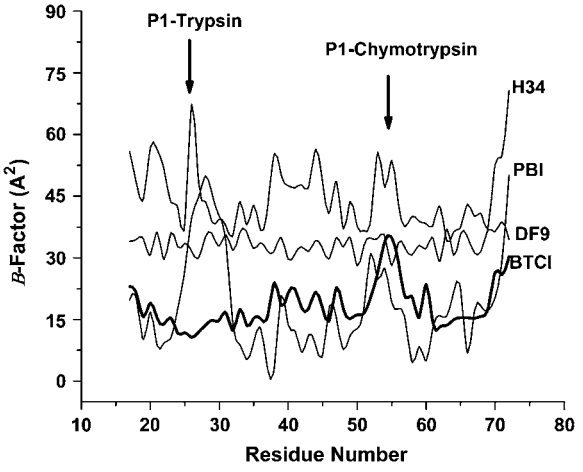

FIGURE 2 B-factor plot for BBIs crystallographic models indicated by their PDB code. The average B-factor for all atoms in each residue is plotted as a function of residue number of BTCI. P1 residues (Lys^{26} and Phe^{53}) are indicated, as antitryptic and antichymotriptic reactive site, respectively.

TABLE 2 Polar contacts between BTCI, trypsin, selected waters, and PEG <3.2 Å apart

	BTCI	Trypsin	Waters	PEG1
P5	Cys^{22}:O	Ser^{217}:OG		
	Cys^{22}:O		W^{132}	
	Cys^{22}:NH		W^{123}	
P4	Glu^{23}:OE1	Gln^{175}:OE1		
	Glu^{23}:OE2		W^{83}	
	Glu^{23}:OE2		W^{73}	
P3	Cys^{24}:NH	Gly^{216}:O		
	Cys^{24}:O	Gly^{216}:NH		
P1	Lys^{26}:NH	Ser^{214}:O		
	Lys^{26}:NH	Ser^{195}:OG		
	Lys^{26}:O	Gly^{193}:NH		
	Lys^{26}:O	Ser^{195}:NH		
	Lys^{26}:O	Ser^{190}:OG		
	Lys^{26}:NZ	Ser^{190}:O		
	Lys^{26}:NZ	Ser^{190}:OG		
	Lys^{26}:NZ	Asp^{189}:OD2		
	Lys^{26}:NZ		W^{2}	
	Lys^{26}:NZ		W^{3}	
		Gly^{219}:O	W^{3}	
		Asp^{189}:OD1	W^{3}	
P1′	Ser^{27}:NH	Ser^{195}:OG		
	Ser^{27}:OG		W^{95}	
P2′	Ile^{28}:NH	Phe^{41}:O		
	Ile^{28}:O	Lys^{60}:NZ		
	Ile^{28}:O		W^{322}	
P3′	Pro^{29}:O		W^{95}	
P4′	Pro^{30}:O		W^{88}	
P5′	Gln^{31}:OE1			19:O
	Gln^{31}:NE2		W^{95}	
	Gln^{31}:NE2		W^{116}	
			W^{71}	19:O
P7′	Arg^{33}:NH1	Ser^{96}:O		
	Arg^{33}:NH2	Asn^{97}:O		
	Arg^{33}:NH2			13:O
	Arg^{33}:NE		W^{103}	
		Gln^{175}:OE1	W^{103}	10:O
			W^{103}	7:O
			W^{323}	7:O
				4:O

The complex structure and its interface

In the crystal, BTCI binds to one molecule of trypsin driven mainly by electrostatic forces with the participation of two water molecules (Fig. 3). The equivalent C_α atoms of trypsin on the refined complex have an RMSD of 0.47 Å compared to those of the initial trypsin model (PDB entry 1TAB), showing that the enzymes' structures in both complexes are closely related. Furthermore, trypsin and the β-hairpin containing the Lys^{26} reactive site are well superimposed, whereas differences are present in the Phe^{53} reactive site (data not shown).

BTCI binds to trypsin primarily at Lys^{26}, the P1 residue (Fig. 3, *a* and *b*), although many other residues participate in

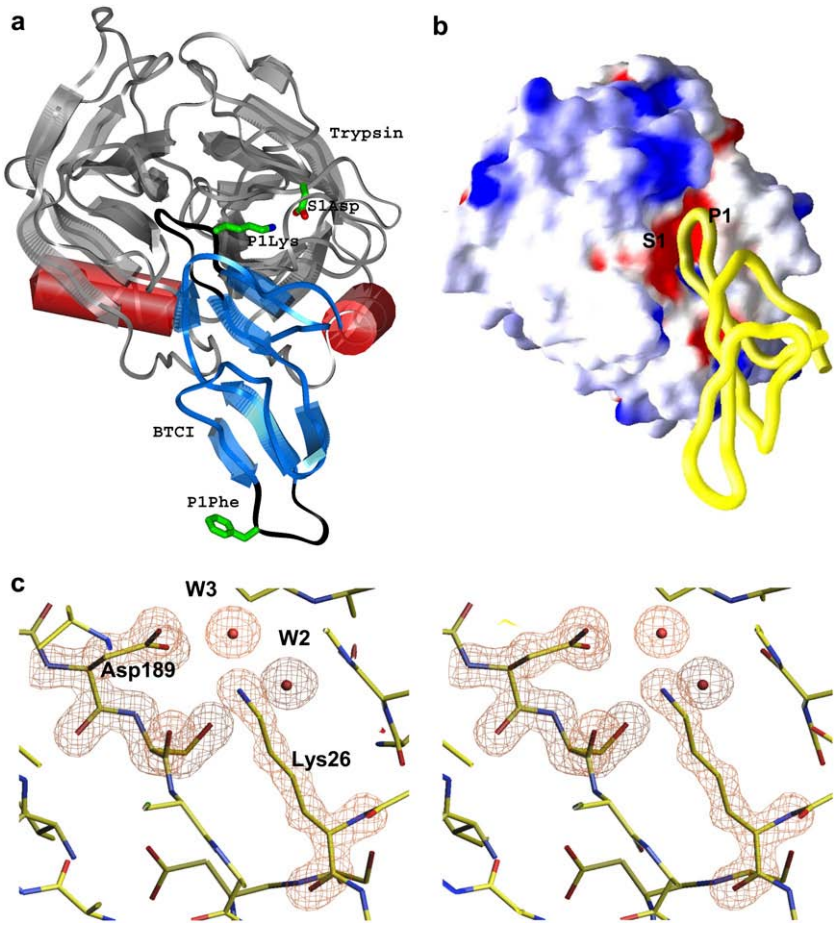

FIGURE 3 (*a*) Overall view of the BTCI-trypsin complex in ribbon representation. Trypsin is shown in gray ribbon, BTCI in blue ribbon, and Lys (P1), Phe (P1), and Asp (S1) residues in stick representation. The reactivity loops of the BTCI are shown in black trace. The extended Lys^{26} side chain is clearly going toward the S1 pocket to interact with Asp^{189}. (*b*) Electrostatic potential surface of trypsin showing the negatively charged (*red*) S1 pocket with a backbone model of BTCI (*yellow tube*) bound (generated with GRASP). (*c*) Stereo view of the BTCI-trypsin complex structure showing simulated annealing omit electron density map contoured at 5.0 σ. Inhibitor's residue Lys^{26}, enzyme's residues Asp^{189} and Ser^{190} and two water molecules were omitted.

the interface. Table 2 summarizes the polar interactions that occur between the two proteins, selected waters, and a PEG molecule. The side chain of Lys^{26} is clearly shown in the electron density map and it is in an extended configuration that perfectly complements the substrate S1 specificity pocket of the enzyme (Fig. 3 *c*). The conformation of this reactive site is maintained by a hydrogen-bond network involving P2 and P1′ exposing the P1 side chain for primary interaction with trypsin (12,15,18). The positively charged amino group at the tip of Lys^{26} is stabilized mainly by the negatively charged Asp^{189} side chain at the trypsin's S1 pocket mediated by the water molecule W3 (Fig. 3 *c*). Another polar contact in the interface includes water molecule, W2, which directly contacts the P1 amino group.

Besides the Lys^{26}-Asp^{189} salt bridge, this protein-protein interface is also characterized by a patchy surface with hydrophobic and hydrophilic side chains (Fig. 4, *a* and *b*). Secondly most important is the hydrogen-bond network between BTCI and trypsin involving the residues and waters listed in Table 2. Weaker hydrophobic interactions, carbon or sulfur atoms separated by <4.5 Å, between the BTCI (Glu^{23}, Thr^{25}, Ser^{27}, Ile^{28}, and Pro^{30}) and trypsin (Tyr^{39}, Phe^{41}, Cys^{42}, His^{57}, Leu^{99}, Tyr^{172}, Cys^{191}, Gln^{192}, Ser^{195}, Val^{213}, Trp^{215}) stabilize the interface. In BTCI, Lys^{26}, Ile^{28}, Glu^{23}, Arg^{33}, and Thr^{25}, listed in decreasing order of interface ASA, correspond to 70% of ASA of the interface that is buried upon complexation, calculated according to Jones and Thornton (52). In the enzyme, the five residues that contribute most for the buried area in the enzyme surface are Glu^{192}, His^{57}, Trp^{215}, Gln^{175}, and Tyr^{39} and reach a total of 44%. These data support the hydrophobic and hydrophilic contacts observed and listed previously.

A PEG molecule from the crystallization solution is also present in the inhibitor-enzyme interface, near the reactive site. The electron density clearly shows six ethylene-glycol units (Fig. 4 *c*). The first four ethylene-glycol units of the PEG are deeply buried within the complex, with the Arg^{33} side chain from BTCI surrounding and preventing its access to the solvent. There are many interactions between the PEG molecule and the proteins. The hydrophilic ones are presented in Table 2, while the hydrophobic ones are with the following residues: Glu^{23}, Cys^{24}, Thr^{25}, Glu^{31}, Arg^{33}, Ser^{35}, Phe^{60}, and Ile^{64} from BTCI and Thr^{98}, Leu^{99}, Glu^{175}, and Trp^{215} from trypsin.

The rigidity of the BBIs has been extensively described and has led to the assumption that these inhibitors do not change their structure upon complexation (21,25). In contrast, De la Sierra et al. (13) proposed that a mobility of

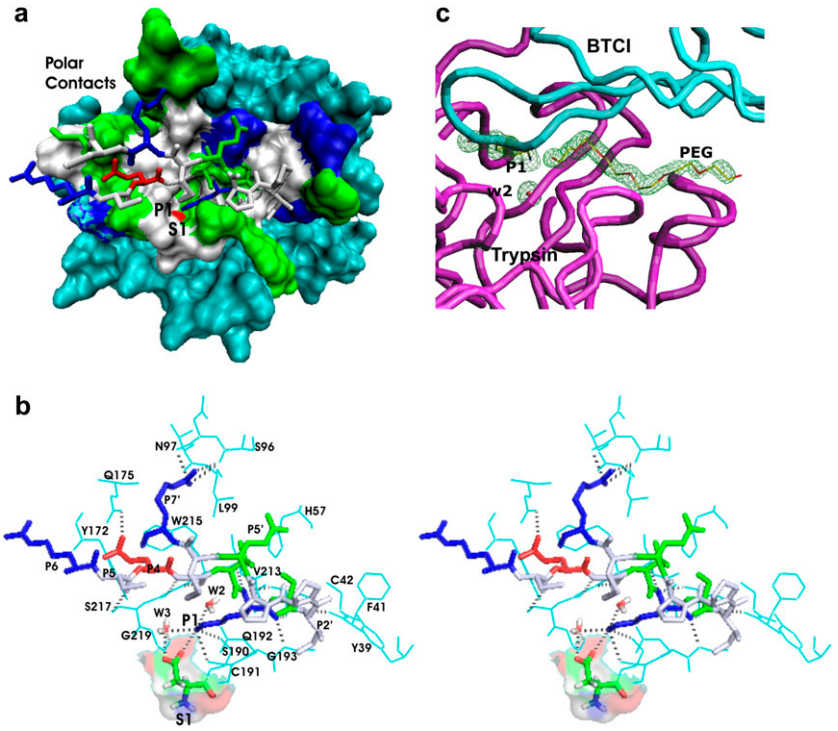

FIGURE 4 Hydrophobic and hydrophilic contacts in the interface of BTCI-trypsin complex. (*a*) Exposed surface area of trypsin is shown in cyan and its buried surface area in close contact with BTCI (amino acids in stick representation) is shown in green (polar residues), white (hydrophobic residues), and blue and red (positively and negatively charged residues). The Asp^{189} (in *red*) is seen only partially deeply buried in the S1 cleft and the reactive site of the BTCI (P1 Lys^{26}) is seen projected into the S1 cleft. (*b*) Stereo-view in the same orientation as in panel *a* showing specific interactions listed in Table 2 generated with PyMOL (53). (*c*) The PEG molecule participating in the stabilization of the complex inside an omit map contoured at 4.2 σ. BTCI and trypsin are colored in light blue and magenta, respectively. The P1 residue is also shown.

reactive loops 1 and 2, relative to each other, is necessary for the precise adjustment of the two enzymes to the inhibitor. In addition, Catalano et al. (14) found that the lack of interdomain disulfide bond allows for flexibility of the spatial orientation of the two domains relative to each other. Koepke et al. (20) has shown by a ternary crystallographic complex between soybean BBI and two trypsin molecules that the conformation of side chains can change dramatically at the reactive loop responsible for chymotrypsin binding. In this case, the additional binding site for trypsin seemed to be located in the chymotrypsin reactive domain. Although it is unclear whether the reactive loop would change if bound to its specific target (chymotrypsin), the conformational changes are possible. This led to the suggestion that the predominance of hydrophilic contacts (as also shown for BTCI in Table 2) and the conformational rigidity of the reactive loop are responsible for the high specificity for trypsin, while high hydrophobicity and significant conformational mobility typical of antichymotryptic subdomain confer a broad inhibition specificity and the self-association tendency. Furthermore, at higher inhibitor concentration the reactive subdomain of soybean BBI is masked from interacting with trypsin by self-association via their chymotrypsin inhibitor site. In the case of the BTCI, the conformational changes could not be ascertained by crystallography since the BTCI-chymotrypsin complex did not crystallize in any conditions tested to date. Furthermore, there are no crystallographic structures of complexes between BBIs and chymotrypsin available in the PDB. These facts were addressed by additional investigation regarding the role of the specific association of the BTCI in the ternary complex using an AFM approach. AFM has the innate capability to accurately resolve, at nearly physiological conditions, the structures and subunit stoichiometries of proteins. It becomes therefore possible to visualize heterogeneous oligomerization processes leading to more than one kind of complex.

Oligomerization state of BTCI-proteinases binary complexes

BTCI incubated with chymotrypsin and trypsin forms binary and ternary complexes with a ratio of 1:1 and 1:1:1, respectively, and these assemblies were imaged by AFM as presented in Fig. 5, *a* and *b*, and Fig. 6 *a*. In this study, oligomerization processes of the above-mentioned binaries and ternary structures were considered based on volumetric parameters. According to our previous studies, this strategy is a much better indicative of the real protein oligomerization state than linear measurements (39). The calculated volumes of trypsin, chymotrypsin, and BTCI monomers were 19 ± 4, 20 ± 4, and 10 ± 5 nm^3, respectively. AFM-determined volumes of BTCI-proteinases complexes were compared with VADAR volumes for proteins present in a typical molecular mass calibration mixture based on three-dimensional coordinates and displayed good agreement (Fig. 7). They correlate well for most molecular mass ranges and some small discrepancy could be clearly associated with solvation aspects used during VADAR algorithm with the Voronoi method.

Molecular volumes and equilibrium constants of the binary and ternary complexes formation were determined

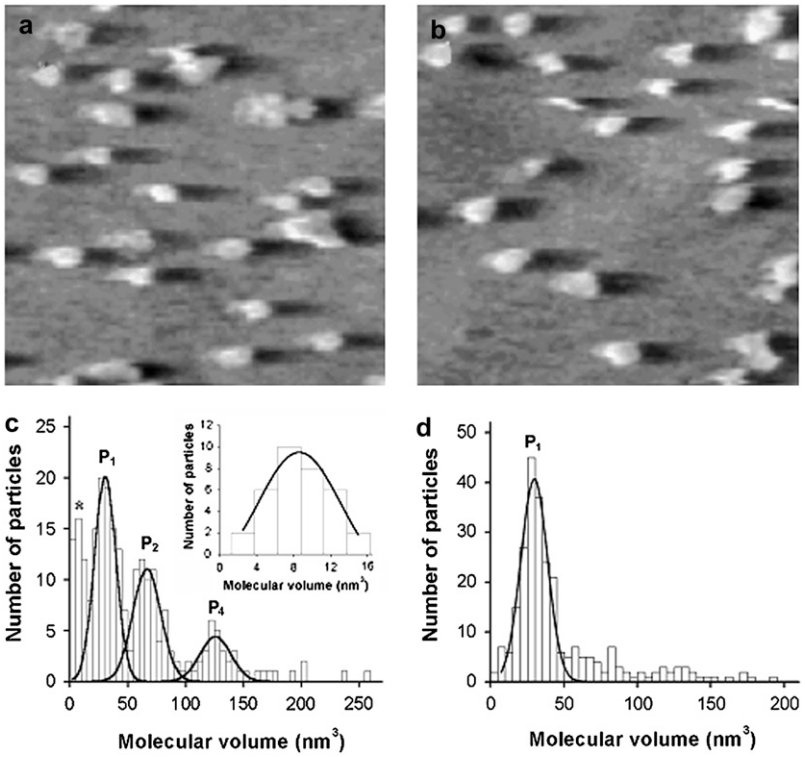

FIGURE 5 (*a*) Topograph of the BTCI-chymotrypsin complex with a full frame of 150 nm^2. Full gray-level range of the topograph corresponds to 3.13 nm. (*b*) Topograph of the BTCI-trypsin complex with a full frame of 150 nm^2. Full gray-level range of the topograph corresponds to 3.04 nm. (*c*) Gaussian fit of the AFM volume histograms for BTCI-chymotrypsin. The solid lines are Gaussian fits of the individual multimeric states. Some volume areas were undefined by Gaussian fit, indicated by *. P_1, P_2, and P_4 correspond to monomer, dimer, and tetramer of the complex, respectively. (*d*) Gaussian fit (P_1) of the AFM volume histograms for BTCI-trypsin. The solid line is the Gaussian fit of the individual monomer.

from a number (n) of particles represented by AFM images used to characterize the particles subfamily cluster (Table 3). Fig. 5, *c* and *d*, and Fig. 6 *b* show the molecular volumes for BTCI-chymotrypsin ($n = 210$) and BTCI-trypsin ($n = 236$), and the ternary complex, chymotrypsin-BTCI-trypsin ($n = 562$), respectively, fitted by Gaussian distributions. For the BTCI-chymotrypsin complex, three main peaks at 31 ± 8 nm^3 ($n = 78$), 67 ± 9 nm^3 ($n = 57$), and 126 ± 8 nm^3 ($n = 25$)

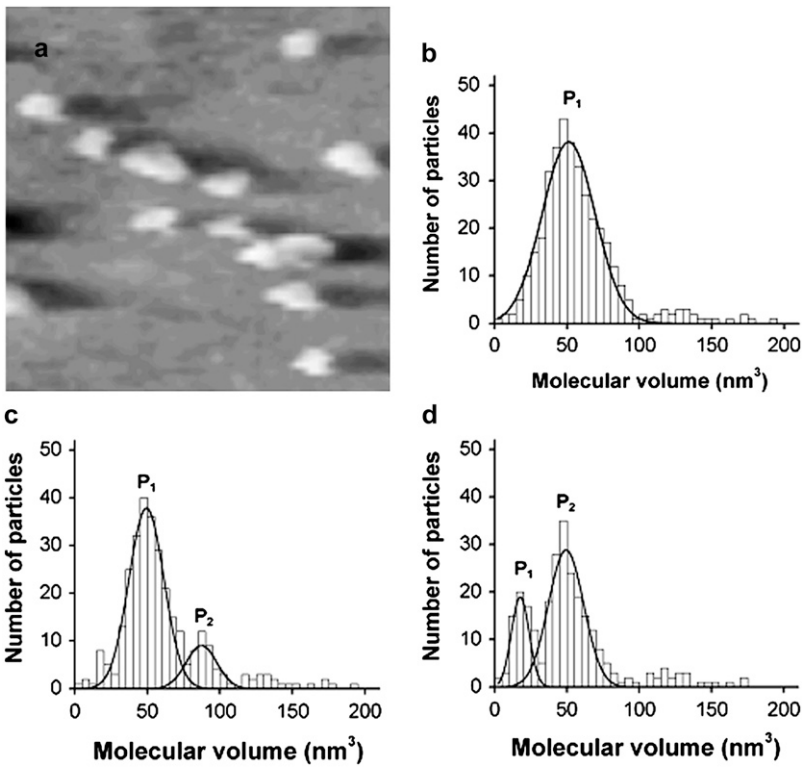

FIGURE 6 (*a*) Topograph of the chymotrypsin-BTCI-trypsin ternary complex with a full frame of 150 nm^2. Full gray-level range of the topograph corresponds to 4.13 nm. (*b*) Gaussian fit AFM volume histograms for purified chymotrypsin-BTCI-trypsin. (*c*) Gaussian fit of the AFM volume histograms for chymotrypsin-BTCI-trypsin obtained by mixing BTCI-chymotrypsin binary complex with trypsin. The solid lines are Gaussian fits of the individual multimeric states. P_1 and P_2 correspond to monomer and an unidentified array of the complex, respectively. (*d*) Gaussian fit of the AFM volume histograms for trypsin-BTCI-chymotrypsin obtained by mixing the BTCI-trypsin binary complex with chymotrypsin. The solid lines are Gaussian fits of the individual multimeric states. P_1 and P_2 correspond to free α-chymotrypsin and the monomer of the ternary complex, respectively.

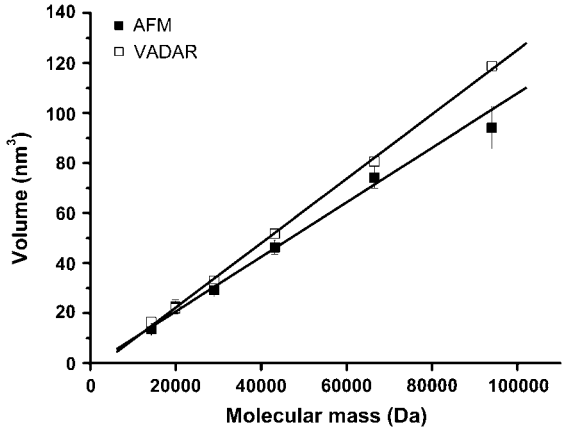

FIGURE 7 Correlation between the molecular mass and volume of the molecular marker proteins (α-lactalbumin, soybean trypsin inhibitor, carbonic anhydrase, ovalbumin, albumin, and phosphorylase b) obtained by AFM and VADAR. Good correlation (within error) could be observed for molecular masses <66 kDa.

(Fig. 5 *c*, Table 3) were obtained after correction for the experimentally measured particles. These peaks were consistent to the monomer (P1), dimer (P2), and tetramer (P4) of the binary association, respectively. The smaller particles (minor peak at 9 ± 4 nm^3 ($n = 34$), indicated by (*) in the Fig. 5 *c* (*inset*) corresponds to the molecular volume of the BTCI monomer, as previously determined by AFM (39). These results suggest that on the 1:1 molar ratio between BTCI and chymotrypsin, the presence of a small amount of dissociated BTCI could be resultant of the proteinase and/or inhibitor self-association tendencies by forming their specific homo multimers. The light-scattering data also support such self-association tendency of BTCI (38).

For BTCI-trypsin and chymotrypsin-BTCI-trypsin, uniformly well-defined line-fitted Gaussian peaks at 30 ± 8 nm^3 ($n = 156$) and at 51 ± 18 nm^3 ($n = 527$), respectively, were observed in the histograms of the volume distribution (Figs. 5 *d* and 6 *b*). These results indicate that the BTCI-trypsin and chymotrypsin-BTCI-trypsin complexes formation is more favored than homo multimers' self-association. The self-association tendency observed for BTCI-chymotrypsin complex displaying several populations of particles (Fig. 5 *c*) and uniform hetero complex population for BTCI-trypsin complex (Fig. 5 *d*) can help to explain the differences in the crystallization processes of these complexes. These observations confirm the importance of AFM to optimize crystallization procedures indicating the circumstances that might permit crystal growth (61).

TABLE 3 AFM-determined Gaussian-fitted molecular parameters evaluated for proteins and their complexes

	Vol. (nm^3)	Ratio*	Freq. (%)	K_{eq}
BTCI[†]	10 ± 5	—	22	—
Dimer	22 ± 6	2.2	16	0.0340
Trimer	34 ± 5	3.4	11	0.0320
Hexamer	69 ± 7	6.9	22	0.1740
BTCI-α-chymotrypsin	31 ± 8	—	37	0.0149
Dimer	67 ± 9	2.2	27	0.0194
Tetramer	126 ± 8	4.1	12	0.0164
BTCI-trypsin	30 ± 8	—	66	0.0264
Ternary (purified)	51 ± 18	—	93	—
BTCI-chymotrypsin + trypsin	49 ± 12	—	76	0.0302
Unknown species[‡]	87 ± 11	1.8	16	—
BTCI-trypsin + chymotrypsin	49 ± 12	—	68	0.0270
Unknown species[§]	18 ± 6	—	22	—
Chymotrypsin	20 ± 4	—	52	—
Dimer	41 ± 4	2.1	24	0.0024
Trimer	63 ± 5	3.1	17	0.0008
Tetramer	82 ± 3	4.1	4	0.0071
Trypsin	19 ± 4	—	65	—
Tetramer	75 ± 3	3.9	24	0.0024

*Oligomer/monomer ratio.
[†]BTCI parameters previously determined (39).
[‡]Unidentified molecular structure.
[§]Unidentified molecular structure with molecular volume related to the dissociated chymotrypsin.

BTCI-proteinases ternary complexes features

Considering that in solution, the ternary complex must be generated by an initial step of binary complex formation, the ternary moiety was also obtained according to the probable following schemes of the association: BTCI-chymotrypsin plus free trypsin or BTCI-trypsin plus free chymotrypsin assemblies. In AFM experimental approaches, the equilibrium between the different visualized forms (Fig. 6, *c* and *d*, respectively) were analyzed and distinct structural features upon binding were observed. The structures related to the ternary complex formed from BTCI-chymotrypsin plus free trypsin association displayed two line-fitted Gaussian peaks at 49 ± 12 nm^3 ($n = 347$) and at 87 ± 11 nm^3 ($n = 73$) (Fig. 6 *c*). Despite the presence of an unidentified species at 87 ± 11 nm^3, there is no evidence of reminiscent building assembly of BTCI-chymotrypsin or free trypsin. On the other hand, the moieties related to the ternary complex formed from BTCI-trypsin plus free chymotrypsin displayed line-fitted Gaussian-peak at 18 ± 6 nm^3 ($n = 88$) and at 49 ± 12 nm^3 ($n = 267$) (Fig. 6 *d*). In this case, the observed reminiscent building assemblies (chymotrypsin molecules at 18 ± 6 nm^3) suggest that a BTCI conformational change may occur upon binding with trypsin or the self-association tendency of chymotrypsin prevent the complete conversion to the ternary form. As previously reported, the ultraviolet difference spectra arise, in the absorption region of the aromatic residues, when BTCI interacts with trypsin or chymotrypsin to form the respective binary complex (62,63). These spectra reflect that the enzyme-inhibitor interaction is accompanied by changes in the environment of the enzyme-inhibitor system. The also expected but not visualized presence of reminiscent BTCI-trypsin molecules may be due to no well-defined Gaussian peaks between P1 and P2 peaks (Fig. 6 *d*).

Proteinases self-association

Although BTCI-proteinases complexes themselves could explain structural aspects of the protein-protein association, the following remarkable question concerning the self-association tendency related to biological function remained as an argument field: which structural attributes contribute to the presence of dissociated forms from ternary complex formation based on BTCI-trypsin plus free chymotrypsin, as shown in Fig. 6 *d*. Factors such as self-association tendency between chymotrypsin molecules, net charge balance changes, or binding-related conformational changes and the flexibility of the reactive site for chymotrypsin could contribute to this unexpected feature. These speculative features were reinforced by the previous finding of the conformational changes in the environment of the enzyme-inhibitor system (62,63) and by the calculated binding constants for trypsin and chymotrypsin to BTCI-proteinase complexes as discussed in the following section.

To investigate the possible role of the described self-association of proteinases, molecular volume determinations from AFM images of the purified chymotrypsin and trypsin were analyzed (Fig. 8, *a* and *b*). Line-fitted Gaussian peaks showed in Fig. 8, *c* and *d*, reveal the volumetric values consistent to monomeric forms of chymotrypsin (20 $\pm$ 4 nm^3, $n = 277$) and trypsin (19 $\pm$ 4 nm^3, $n = 273$), respectively, that are in agreement with molecular volumes calculated by VADAR (Fig. 7). However, the additional peaks also reveal the proteinases' self-association tendency. In the case of chymotrypsin (Fig. 8 *c*) the observed schemes of association were consistent to dimers (41 $\pm$ 4 nm^3, $n = 129$), trimers (63 $\pm$ 5 nm^3, $n = 91$), and tetramers (82 $\pm$ 3 nm^3, $n = 22$); whereas, in the case of trypsin, only tetramers (75 $\pm$ 3 nm^3, $n = 100$) were observed (Fig. 8 *d*). Smaller particles, indicated by * in Fig. 8 *c*, probably correspond to the molecular volume of dissociated subunits of chymotrypsin monomer or autodigestion. It has been well recognized that several enzymes involved in biochemical pathways associate to form multienzyme complexes. This feature still remains as a controversy since some research groups hypothesize that there is no structural or functional gain upon self-association and others researchers believe that proteinase self-association tendency leads to some biological advantage in the enzymatic reaction. Our findings showed that close-related enzymes (chymotrypsin and trypsin) have distinct tendencies of multicomplex formation. It may represent a specific and distinct way that allows substrates (or substrate mimicking, like inhibitors) to efficiently access the active sites. In case of chymotrypsin, it has been recently recognized that the oligomerization has a crucial role for determining the affinity and specificity of inhibitors (64). They have demonstrated that the binding energy for turkey ovomucoid third subdomain and chymotrypsin association is close to the coupled monomer-dimer equilibrium of chymotrypsin. In the present AFM study, we have evidence that in addition to dimers, trimers and tetramers could also contribute in a minor extent to the final binding energetic balance.

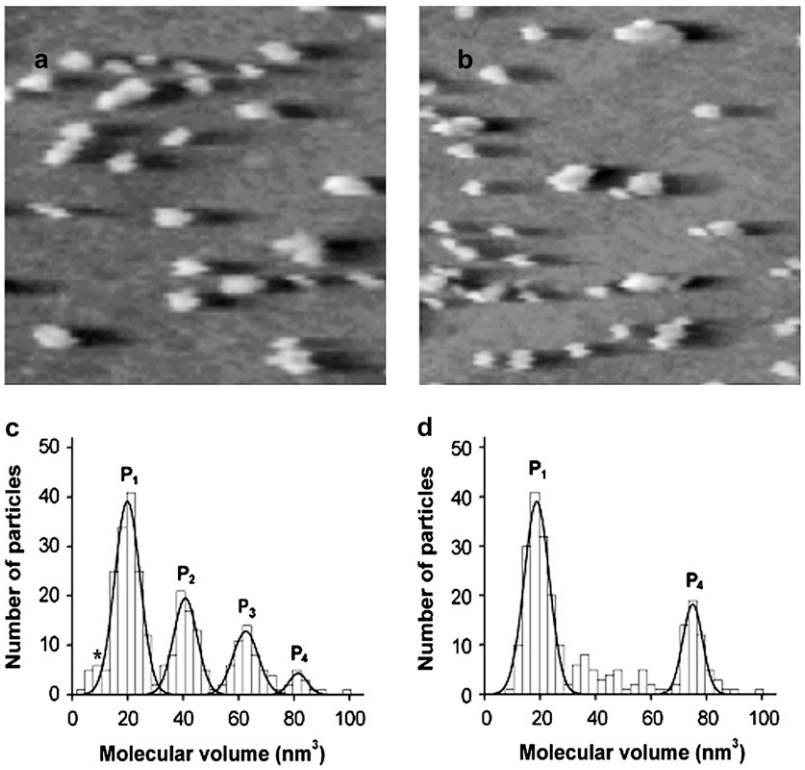

FIGURE 8 (*a*) Topograph of the α-chymotrypsin with a full frame of 150 nm^2. Full gray-level range of the topograph corresponds to 2.57 nm. (*b*) Topograph of the trypsin with a full frame of 150 nm^2. Full gray-level range of the topograph corresponds to 2.42 nm. (*c*) Gaussian fit of the AFM volume histograms for chymotrypsin. The solid lines correspond to the individual multimeric states. Volume areas undefined by Gaussian fit were indicated by *. P_1, P_2, P_3, and P_4 correspond to monomer, dimer, trimer, and tetramer of the protein, respectively. (*d*) Gaussian fit of the AFM volume histograms for trypsin. The solid lines are Gaussian fits of the individual multimeric states. Some volume areas were undefined by Gaussian fit. P_1, and P_4 correspond to monomer, and tetramer of the protein, respectively.

Proteinase binding in a ternary complex

In an attempt to rationalize the AFM findings, we investigated the proteinase-inhibitor binding properties of the BTCI-trypsin complex with chymotrypsin and of the BTCI-chymotrypsin complex with trypsin. As has been shown, BTCI displays ~10-fold more affinity for the trypsin ($K_i = 2 \times 10^{-8}$ M) than chymotrypsin ($K_i = 1.2 \times 10^{-7}$ M) (32,33). In this study, we found that when BTCI is in the binary forms with chymotrypsin or trypsin, the affinity of this inhibitor for producing a ternary complex shows no significant differences. The inhibition constants (K_i) for each binary complex against trypsin and chymotrypsin, calculated from fitted inhibition curves (Fig. 9), were $1.36 \pm 0.16 \times 10^{-8}$ M and $1.13 \pm 0.34 \times 10^{-7}$ M, respectively. These results suggest that when BTCI is in binary complex with trypsin and chymotrypsin it presents no conformational change of the specific reactive site for both enzymes. This result corroborates that both reactive sites are structurally independent. Therefore, the free chymotrypsin observed in the AFM assays (Fig. 6 *d*), when the ternary complex is obtained (Fig. 6 *d*, P2) by mixing BTCI-trypsin binary complex with chymotrypsin, could be related more to the self-association tendency between chymotrypsin molecules and the flexibility of the reactive site for chymotrypsin than to binding-related conformational changes.

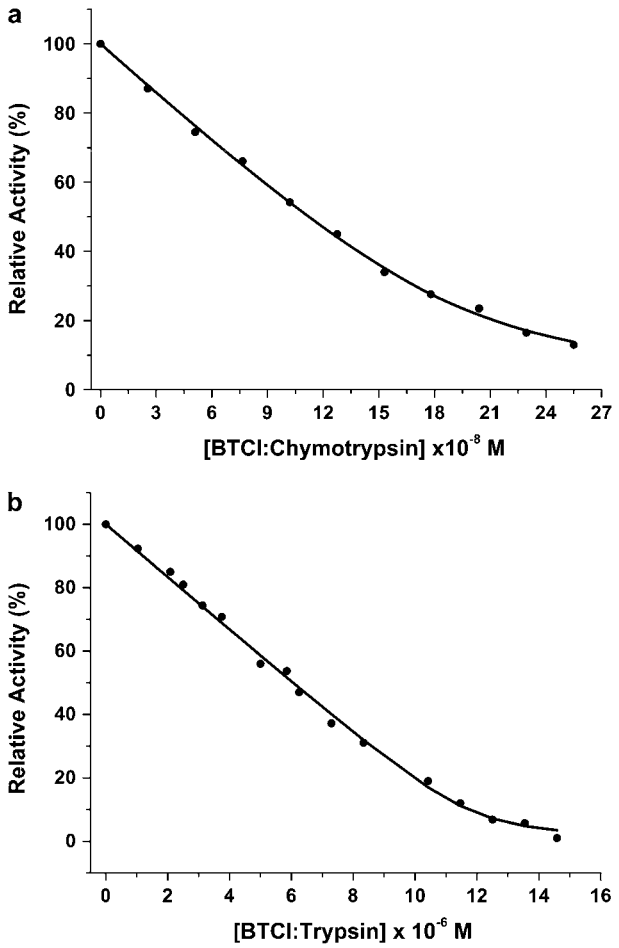

FIGURE 9 (*a*) Inhibitory activities of BTCI-chymotrypsin complex toward bovine pancreatic trypsin. The inhibition constant, calculated from the fitted curve, was $1.36 \pm 0.16 \times 10^{-8}$ M. (*b*) Inhibitory activity of BTCI-trypsin complex toward bovine pancreatic chymotrypsin. The inhibition constant, calculated from the fitted curve, was $1.13 \pm 0.34 \times 10^{-7}$ M.

As previously demonstrated, the enzyme inhibitor interaction is accompanied by changes in the environment of the aromatic chromophores of the BTCI-proteinase system (62,63). The oxidation of tryptophyl residues with *n*-bromosuccinimide indicated an involvement of such residues in the interaction of the inhibitor with trypsin or chymotrypsin (63). The interaction between trypsin and BTCI results in the burying of the equivalent to approximately one tryptophyl group. It was assumed that in the formation of the ternary complex, the burying of tryptophyl, which results from the interaction of trypsin with BTCI, is counteracted by the opposite effect resulting from the interaction with chymotrypsin (62). In agreement with this results, the crystallographic structure of the BTCI-trypsin shows that the only tryptophyl residue buried in the interface is Trp^{215} from the enzyme (Fig. 4 *b*).

These results show that BBIs present independent reactive sites and the conformational changes upon binary and ternary complexes formation are on the interface of the complexes. Despite the identified differences in the self-association features, the relationship between the structure and its biological implications still remains as an open question, especially due to the lack of the structures of the BTCI-chymotrypsin and ternary complex involving BBIs, trypsin, and chymotrypsin molecules. However, even though BTCI is a rigid molecule with high disulfide bond content, the structure displacement of the antichymotryptic subdomain relative to antitryptic subdomain cannot be discarded, as previously reported for BBI from pea seeds (13). Indeed, as indicated by the crystal BTCI-trypsin complex, the antichymotryptic subdomain displays higher flexibility and hydrophobicity with respect to the antitryptic subdomain, and these properties could be correlated to the self-association AFM findings. It is noteworthy that the difference between the stable BTCI-trypsin complex with low flexibility and the BTCI-chymotrypsin complex with a flexible reactive site was also seen in the ternary complex of soybean BBI (20). This is in agreement with the reported self-association of subdomain 2 of BBIs that has been suggested to protect it from enzyme attack (11,13,29,30). The chymotrypsin inhibitory subdomain in a soybean proteinase inhibitor (11) presents various crystal contacts between molecules structurally organized in trimers indicating that the antichymotryptic subdomain is responsible for this self-association. Indeed, the self-association involves charged and hydrophobic residues at subdomain 2 indicating that electrostatic and hydrophobic intermolecular interactions are the driving forces for inhibitors association

(14,20,30). This self-association, together with the other discussed structural aspects, accounts for the structural stability of the BBIs and indicates a functional and relevant aspect of the self-association process with a possible involvement of this subdomain in interactions with other enzymes or macromolecules.

This study shows that BTCI has a similar structural arrangement to other BBIs as expected. This group of proteins has three major roles recognized for them: the regulation of endogenous seed proteinases, the storage of sulfur amino acids, and the defense against pathogens and insect attack by an antidigestive effect inhibiting the proteolysis process. The described self-association tendency of BTCI can relate to its function in storage since affinity for itself is a requirement for the molecular packing in the plant seeds. Also, our results support that the reactive sites of double-headed inhibitors belonging to the BBIs are structurally independent motifs, being able to bind and inhibit both enzymes at the same time. Furthermore, although it seems that the distribution of chymotrypsin-like enzymes among insects is similar to that of trypsin, midgut chymotrypsin-like activity is usually low in *Lepidoptera* (65). This agrees with our findings since the BTCI interaction with trypsin is stronger than with chymotrypsin, leading to the suggestion that proteinases and their inhibitors could be implicated in a coevolutionary process.

COORDINATES

The atomic coordinates have been deposited in the RCSB Protein Data Bank, and were given the code number 2G81.

We thank the Brazilian Synchrotron Light Laboratory and Dr. Marcelo V. de Sousa for analysis of some ambiguous amino acids in the BTCI sequence.

We gratefully acknowledge the financial support of Conselho Nacional de Desenvolvimento Científico e Tecnológico (CNPq) (grant No. 476509/2003-3 and grant No. 480121-02-8, ReNaBiME program).

REFERENCES

1. Laskowski, M., Jr., and I. Kato. 1980. Protein inhibitors of proteinases. *Annu. Rev. Biochem. Rev.* 49:593–626.
2. Bode, W., and R. Huber. 2000. Structural basis of the endoproteinase-protein inhibitor interaction. *Biochim. Biophys. Acta.* 7:241–252.
3. Laskowski, M., and M. A. Qasim. 2000. What can the structures of enzyme-inhibitor complexes tell us about the structures of enzyme substrate complexes? *Biochim. Biophys. Acta.* 1477:324–337.
4. Mello, M. O., A. S. Tanaka, and M. C. Silva-Filho. 2003. Molecular evolution of Bowman-Birk type proteinase inhibitors in flowering plants. *Mol. Phylogenet. Evol.* 27:103–112.
5. Kato, G. J. 1999. Human genetic diseases of proteolysis. *Hum. Mutat.* 13:87–98.
6. Ryan, C. A. 1991. Proteinase inhibitors in plants: genes for improving defenses against insects and pathogens. *Annu. Rev. Phytol.* 28:425–449.
7. Franco, O. L., R. C. dos Santos, J. A. N. Batista, A. C. M. Mendes, M. A. de Araújo, R. G. Monnerat, M. F. Grossi-de-Sá, and S. M. de Freitas. 2003. Effects of black-eyed pea trypsin/chymotrypsin inhibitor on proteolytic activity and on development of *Anthonomus grandis*. *Phytochemistry.* 63:343–349.
8. Kennedy, A. R. 1998. The Bowman-Birk inhibitor from soybean as an anticarcinogenic agent. *Am. J. Clin. Nutr.* 68:1406–1412.
9. Chen, P., J. Rose, R. Love, C. H. Wei, and B. C. Wang. 1992. Reactive sites of an anticarcinogenic Bowman-Birk proteinase inhibitor are similar to other trypsin inhibitors. *J. Biol. Chem.* 267:1990–1994.
10. Suzuki, A., T. Yamane, T. Ashida, S. Norioka, S. Hara, and T. Ikenazka. 1993. Crystallographic refinement of Bowman-Birk type protease inhibitor A-II from peanut (*Arachis hypogaea*) at 2.3 Å resolution. *J. Mol. Biol.* 234:722–734.
11. Werner, M. H., and D. E. Wemmer. 1992. Three-dimensional structure of soybean trypsin/chymotrypsin Bowman-Birk inhibitor in solution. *Biochemistry.* 31:999–1010.
12. Voss, R. H., U. Ermler, L. O. Essen, G. Wenzl, Y. M. Kim, and P. Flecker. 1996. Crystal structure of the bifunctional soybean Bowman-Birk inhibitor at 0.28 nm resolution. Structural peculiarities in a folded protein conformation. *Eur. J. Biochem.* 242:122–131.
13. De la Sierra, I., L. Quillien, P. Flecker, J. Gueguen, and S. Brunie. 1999. Dimeric crystal structure of a Bowman-Birk protease inhibitor from pea seeds. *J. Mol. Biol.* 285:1195–1207.
14. Catalano, M., L. Ragona, H. Molinari, A. Tava, and L. Zetta. 2003. Anticarcinogenic Bowman Birk inhibitor isolated from snail medic seeds (*Medicago scutellata*): solution structure and analysis of self-association behavior. *Biochemistry.* 42:2836–2846.
15. Song, H. K., Y. S. Kim, J. K. Yang, J. Moon, J. Y. Lee, and S. W. Suh. 1999. Crystal structure of a 16 kDa double-headed Bowman-Birk trypsin inhibitor from barley seeds at 1.9 Å resolution. *J. Mol. Biol.* 293:1133–1144.
16. Debreczeni, J., G. Bunkoczi, B. Girmann, and G. Sheldrick. 2003. In-house phase determination of the lima bean trypsin inhibitor: a low-resolution sulfur-SAD case. *Acta Crystallogr. Sect. D.* 59:393–395.
17. Tsunogae, Y., I. Tanaka, T. Yamane, J. Kikkawa, T. Ashida, C. Ishikawa, K. Watanabe, S. Nakamura, and K. Takahashi. 1986. Structure of the trypsin-binding domain of Bowman-Birk type protease inhibitor and its interaction with trypsin. *J. Biochem.* (*Tokyo*). 100: 1637–1646.
18. Lin, G., W. Bode, R. Huber, C. W. Chu, and R. A. Engh. 1993. The 0.25 nm x-ray structure of the Bowman-Birk type inhibitor form mung bean in ternary complex with porcine trypsin. *Eur. J. Biochem.* 212: 549–555.
19. Li, Y., Q. Huang, S. Zhang, S. Liu, C. Chi, and Y. Tang. 1994. Studies on an artificial trypsin inhibitor peptide derived from the mung bean trypsin inhibitor: chemical synthesis, refolding, and crystallographic analysis of its complex with trypsin. *J. Biochem.* (*Tokyo*). 116:18–25.
20. Koepke, J., U. Ermler, E. Warkentin, G. Wenzl, and P. Flecker. 2000. Crystal structure of cancer chemopreventive Bowman-Birk inhibitor in ternary complex with bovine trypsin at 2.3 Å resolution. Structural basis of Janus-faced serine protease inhibitor specificity. *J. Mol. Biol.* 298:477–491.
21. Murthy, H. M., K. Judge, L. DeLucas, and R. Padmanabhan. 2000. Crystal structure of dengue virus NS3 protease in complex with a Bowman-Birk inhibitor: implications for flaviviral polyprotein processing and drug design. *J. Mol. Biol.* 301:759–767.
22. Park, E. Y., J. A. Kim, H. W. Kim, Y. S. Kim, and H. K. Song. 2004. Crystal structure of the Bowman-Birk inhibitor from barley seeds in ternary complex with porcine trypsin. *J. Mol. Biol.* 343:173–186.
23. Freitas, S. M., L. V. de Mello, M. C. da Silva, G. Vriend, G. Neshich, and M. M. Ventura. 1997. Analysis of the black-eyed pea trypsin and chymotrypsin inhibitor-α-chymotrypsin complex. *FEBS Lett.* 409: 121–127.
24. Gaier, J. R., A. Tulinsky, and I. E. Liener. 1981. Formation, crystallization, and preliminary crystallographic data of the ternary complex of α-chymotrypsin, β-trypsin, and the Bowman-Birk inhibitor. *J. Biol. Chem.* 256:11417–11419.
25. Bode, W., and R. Huber. 1992. Natural protein proteinase inhibitors and their interaction with proteinases. *Eur. J. Biochem.* 204:433–451.
26. Liu, J., Y. Gong, O. Prakash, L. Wen, I. Lee, J. K. Huang, and R. Krishnamoorthi. 1998. NMR studies of internal dynamics of serine

proteinase protein inhibitors: binding region mobilities of intact and reactive-site hydrolyzed *Cucurbita maxima* trypsin inhibitor (CMTI)-III of the squash family and comparison with those of counterparts of CMTI-V of the potato I family. *Protein Sci.* 7:132–141.

27. Odani, S., and T. Ikenaka. 1978. Studies on soybean trypsin inhibitors. XIII. Preparation and characterization of active fragments from Bowman-Birk proteinase inhibitor. *J. Biochem.* (*Tokyo*). 83:747–753.
28. Gennis, L. S., and C. R. Cantor. 1976. Double-headed protease inhibitors from black-eyed peas. III. Subunit interaction of the native and half site chemically modified proteins. *J. Biol. Chem.* 251:747–753.
29. Terada, S., S. Fujimura, S. Kino, and E. Kimato. 1994. Purification and characterization of three proteinase inhibitors from *Canavalia lineata* seeds. *Biosci. Biotechnol. Biochem.* 58:371–375.
30. Kumar, P. A. G., A. Rao, S. Hariharaputran, N. Chandra, and L. R. Gowda. 2004. Molecular mechanism of dimerization of Bowman-Birk inhibitors—pivotal role of ASP^{76} in the dimerization. *J. Biol. Chem.* 279:30425–30432.
31. Xavier-Filho, J., and M. M. Ventura. 1988. Trypsin inhibitors in Cowpea: a review. *Comments Agric. Food Chem.* 1:239–314.
32. Fachetti, H. C. S., K. Mizuta, and M. M. Ventura. 1984. Thermodynamics of the black-eyed pea trypsin and chymotrypsin inhibitor. *An. Acad. Bras. Cienc.* 56:311–317.
33. Freitas, S. M., H. Ikemoto, and M. M. Ventura. 1999. Thermodynamics of the binding of chymotrypsin with the black-eyed pea trypsin and chymotrypsin inhibitor (BTCI). *J. Protein Chem.* 18:307–313.
34. Silva, L. P., J. R. S. A. Leite, C. Bloch, Jr., and S. M. de Freitas. 2001. Stability of a black eyed pea trypsin/chymotrypsin inhibitor (BTCI). *Prot. Pept. Lett.* 8:33–38.
35. Morhy, L., and M. M. Ventura. 1987. The complete amino acid sequence of the *Vigna unguiculata* (L.) WaLP seed trypsin and chymotrypsin inhibitor. *An. Acad. Bras. Cienc.* 59:71–81.
36. Ventura, M. M., C. O. Martin, and L. Morhy. 1975. A trypsin and chymotrypsin inhibitor form black-eyed pea (*Vigna sinensis* L.). VI. Isolation and properties of complexes with trypsin and chymotrypsin. *An. Acad. Bras. Cienc.* 47:335–346.
37. Ventura, M. M., K. Mizuta, and H. Ikemoto. 1984. Solvent perturbation and surface accessibility of the tryptophyl and tyrosyl groups in black-eyed pea trypsin and chymotrypsin inhibitor. *An. Acad. Brasil. Ciênc.* 56:217–220.
38. Ventura, M. M., K. Mizuta, and H. Ikemoto. 1981. Self-association of the black-eyed pea trypsin and chymotrypsin inhibitor in solution. A study by light scattering. *An. Acad. Bras. Cienc.* 53:195–201.
39. Silva, L. P., R. B. Azevedo, P. C. Morais, M. M. Ventura, and S. M. de Freitas. 2005. Oligomerization states of Bowman-Birk inhibitor by atomic force microscopy and computational approaches. *Prot. Struct. Funct. Bioinformat.* 61:642–648.
40. Barbosa, J. A. R. G., R. C. L. Teles, V. P. Forrer, B. G. Guimarães, F. J. Medrano, M. M. Ventura, and S. M. de Freitas. 2003. Crystallization, data collection and phasing of black-eyed pea trypsin/chymotrypsin inhibitor in complex with bovine β-trypsin. *Acta Crystallogr. D.* 59: 1828–1830.
41. Otwinowski, Z., and W. Minor. 1997. Processing of x-ray diffraction data collected in oscillation mode. *Methods Enzymol.* 276:307–326.
42. Jones, T. A., J. Y. Zou, S. W. Cowan, and M. Kjeldgaard. 1991. Improved methods for building protein models in electron density maps and the location of errors in these models. *Acta Crystallogr. A.* 47:110–119.
43. Brünger, A. T., P. D. Adams, G. M. Clore, W. L. DeLano, P. Gros, R. W. Grosse-Kunstleve, J. S. Jiang, J. Kuszewski, M. Nilges, N. S. Pannu, R. J. Read, L. M. Rice, T. Simonson, and G. L. Warren. 1998. Crystallography and NMR system: a new software suite for macromolecular structure determination. *Acta Crystallogr. D.* 54: 905–921.
44. Murshudov, G. N., A. A. Vagin, A. Lebedev, K. S. Wilson, and E. J. Dodson. 1999. Efficient anisotropic refinement of macromolecular structures using FFT. *Acta Crystallogr. D.* 55:247–255.
45. Collaborative Computational Project, Number 4. 1994. The CCP4 Suite: programs for protein crystallography. *Acta Cryst. D.* 50:760–763.
46. Emsley, P., and K. Cowtan. 2004. COOT: model-building tools for molecular graphics. *Acta Crystallogr. D.* 20:2126–2132.
47. Perrakis, A., R. Morris, and V. S. Lamzin. 1999. Automated protein model building combined with iterative structure refinement. *Nat. Struct. Biol.* 6:458–463.
48. Kleywegt, G. J., and T. A. Jones. 1998. Databases in protein crystallography. CCP4 proceedings. *Acta Crystallogr. D.* 54:1119–1131.
49. Laskowski, R. A., M. W. McArthur, D. S. Moss, and J. M. Thornton. 1993. PROCHECK: a program to check the stereochemical quality of protein structures. *J. Appl. Crystallogr.* 26:283–291.
50. Gibrat, J. F., T. Madej, and S. H. Bryant. 1996. Surprising similarities in structure comparison. *Curr. Opin. Struct. Biol.* 6:377–385.
51. Humphrey, W., A. Dalke, and K. Schulten. 1996. VMD—visual molecular dynamics. *J. Mol. Graph.* 14:33–38.
52. Jones, D. T., and J. M. Thornton. 1996. Potential energy functions for threading. *Curr. Opin. Struct. Biol.* 6:210–216.
53. DeLano, W. L. The PyMOL Molecular Graphics System. 2002. DeLano Scientific, San Carlos, CA. http://pymol.sourceforge.net.
54. Nicholls, A., K. Sharp, and B. Honig. 1991. Protein folding and association: insights from the interfacial and thermodynamic properties of hydrocarbons. *Protein Struct. Funct. Genet.* 11:281–296.
55. Leite, J. R. S. A., L. P. Silva, M. I. S. Rodrigues, M. V. Prates, G. D. Brand, B. M. Lacava, R. B. Azevedo, A. L. Bocca, S. Albuquerque, and C. Bloch, Jr. 2005. Phylloseptins: a novel class of anti-bacterial and anti-protozoan peptides from the *Phyllomedusa genus*. *Peptides.* 26:565–573.
56. Willard, L., A. Ranjan, H. Y. Zhang, H. Monzavi, R. F. Boyko, B. D. Sykes, and D. S. Wishart. 2003. VADAR: a web server for quantitative evaluation of protein structure quality. *Nucleic Acids Res.* 31:3316–3319.
57. Erlanger, B. F., N. Kokowsky, and W. Cohen. 1961. The preparation and properties of two new chromogenic substrates of trypsin. *Arch. Biochem. Biophys.* 95:271–278.
58. Martin, C. O., and M. M. Ventura. 1986. Trypsin and chymotrypsin inhibitor of *Vigna unguiculata* seeds—involvement of tyrosyls in its interaction with protease. *An. Acad. Brasil. Ciênc.* 58:297–302.
59. Morrison, J. F. 1982. The slow-binding and slow, tight-binding inhibition of enzyme catalyzed reactions. *Trends Biochem. Sci.* 7:102–105.
60. Burley, S. K., and G. A. Petsko. 1985. Aromatic-aromatic interaction: a mechanism of protein structure stabilization. *Science.* 229:23–28.
61. McPherson, A., Y. G. Kuznetsov, A. J. Malkin, and M. Plomp. 2004. Macromolecular crystal growth investigations using atomic force microscopy. *J. Synchrotr. Rad.* 11:21–23.
62. Morhy, L., and M. M. Ventura. 1978. Accessibility of tryptophyl groups in the black-eyed pea inhibitor and its complexes with β-trypsin and/or α-chymotrypsin. A study by thermal perturbation spectroscopy. *An. Acad. Brasil. Ciênc.* 50:239–248.
63. Ventura, M. M., G. B. Araújo, M. A. H. Cagnin, and C. O. Martin. 1972. A trypsin and chymotrypsin inhibitor from black-eyed pea (*Vigna sinensis* L.) IV. *An. Acad. Brasil. Ciênc.* 44:581–582.
64. Filfil, R., and T. V. Chalikian. 2003. The thermodynamics of protein-protein recognition as characterized by a combination of volumetric and calorimetric techniques: the binding of turkey ovomucoid third domain to α-chymotrypsin. *J. Mol. Biol.* 326:1271–1288.
65. Christeller, J. T., W. A. Laing, N. P. Markwick, and E. P. J. Burgess. 1992. Midgut protease activities in 12 phytophagous *Lepidopteran* larvae: dietary and protease inhibitor interactions. *Insect Biochem. Mol. Biol.* 22:735–746.